

Application No.: 10/761,992

Docket No.: JCLA11796

REMARKS

Applicants respectfully submit that applicant's admitted prior art (hereafter PA) in view of Rhodes et al. (U.S. 2004/0178430; hereafter Rhodes) is legally deficient for the purpose of rendering claims 1-7 unpatentable because the reference or references, taken alone or combined, fails to teach or suggest each and every element recited in the claims. The Applicants have further added claims 12-15 to improve clarity. After entry of the foregoing amendments, claims 1-7 and 12-15 remain pending in the present application, and reconsideration of those claims is respectfully requested.

The Applicant's invention is directed to a method of fabricating an image sensor device. As for the shallow trench isolations formed around the photo sensitive region, there is an anti-reflective layer formed therein to reduce the light reflected from the bottom and the sidewall of the trenches. Therefore, the image sensor device of the present invention reduces light reflection at the bottoms and sidewalls of the shallow trench isolation regions. It means that the area of the effective photo sensitive region of the image sensor device increases, and currents generated at the photo sensitive region is enhanced.

However, the PA fails teach or suggest that an anti-reflective layer is formed in the shallow trench isolation regions to reduce the reflection light from the bottom and the sidewall of the shallow trench isolation regions. Moreover, Rhodes fails to teach or suggest that the thin insulating layer 154 can be used as an anti-reflective layer. Instead, Rhodes emphasizes that the thin insulating layer 154 is formed to aid in smoothing out the corners of stress in the dielectric material used to later fill in the trenches (paragraph [0044]). That is, Rhodes focuses on the

Application No.: 10/761,992

Docket No.: JCLA11796

corner stress problem and solves the problem by using the physical property of the thin insulating layer 154.

“Particular findings must be made as to the reason the skilled artisan, with no knowledge of the claimed invention, would have selected these components for combination in the manner claimed.” In re Kozab, 217 F.3d 1365, 1371 (Fed. Cir. 2000). “In other words, the examiner must show reasons that the skilled artisan, confronted with the same problems as the inventor and with no knowledge of the claimed invention, would select the elements from the cited prior art reference for combination in the manner claimed” In re Rouffet, 149 F.3d 1350, 1357 (Fed. Cir. 1998). Apparently, although Rhodes’ application is with respect to the photodiode, Rhodes never raises the issue of light reflection from the bottom and the sidewall of the trenches. Furthermore, it is well known in the art that the material layer for rounding the corners of the trench is formed under a relatively high temperature so as to change the stress of the corners of the trench. Therefore, the material layer formed under the high temperature formation recipe does not necessary possess the anti-reflective property.

Additionally, in response to the assertion in the Office Action that “the modified invention of Admitted prior art, as modified by the teaching of Rhodes would not have light reflection because nitride acts as anti-reflection layer”, Applicants respectfully submit that the material of the anti-reflective layer is not limited to the nitride material. The spirit of the present invention is to form the material layer with anti-reflective property in the shallow trench isolation regions for blocking the reflection light from the bottom and the sidewall of the trenches. The use of the nitride material for forming the anti-reflective layer in the shallow trench isolation

Application No.: 10/761,992

Docket No.: JCLA11796

regions is one of the examples recited in the present invention. Applicants respectfully submit that it is not proper to analogize the thin insulating layer to be the anti-reflective layer just because some of the selected materials for forming the anti-reflective layer are as same as those for forming the thin insulating layer. Furthermore, as indicated in Exhibit A (B. Kim, S.S. Han, T.S. Kim, B.S. Kim and I.J. Shim, "Modeling Refraction Characteristic of Silicon Nitride Film Deposited in a $\text{SiH}_4\text{-NH}_3\text{-N}_2$ Plasma Using Neural Network", IEEE Transaction on Plasma Science, Vol. 31, No. 3, June 2003), the refraction index of the silicon nitride film varies with the proportion of the NH_3 to the gas mixture of NH_3 and SiH_4 in the plasma for forming the silicon nitride film. That is, while the flow rate of the NH_3 is increased from 220 sccm to 260 sccm at 180 sccm, the silicon nitride film becomes more transparent (page 320, Section C, paragraph 2nd). Apparently, not all the silicon nitride film can be an anti-reflective layer. The key for the silicon nitride film to be an anti-reflective layer depends on the formation recipe of the silicon nitride film. Nevertheless, none of the PA and Rhodes recites that the silicon nitride insulating film is form to be an anti-reflective layer by using specific manufacturing process. "The mere fact that the prior art may be modified in the manner suggested by the Examiner does not make the modification obvious unless the prior art suggested the desirability of the modification." **In re Fritch**, 972 F.2d 1260, 1266, 23 U.S.P.Q.2d 1780 (Fed Cir. 1992). Since not only the PA fails to tech or suggest the formation of the anti-reflective layer in the shallow trench isolation regions but also Rhodes fails to imply that the thin insulating layer 154 can be an anti-reflective layer, Applicants respectfully submit that the modification of the PA by referring to Rhodes' application does not render the present invention obviousness.

Application No.: 10/761,992**Docket No.: JCLA11796**

In light of the amendment and the foregoing discussion, claims 1 is not anticipated by prior art and are believed to be patentably distinguished from the cited art so that the reconsideration and withdrawal of the Office Action's rejection on claim 1 under 35 U.S.C § 103 are respectfully requested. Additionally, claims 2-7 respectively depend from claims 1, so that claims 2-7 are believed patentable based on the above remark.

Newly Added Claims

Applicants have added claims 12-15 for re-defining the present invention by introducing that the anti-reflective layer is formed within the isolation structure. It is believed that no new matter is introduced into the application by adding the new set of claims.

For at least the above reasons that PA in view of Rhodes fails to teach or suggest each element in the claims, Applicants respectfully submit that the combination of PA and Rhodes does not render claims 12-15 unpatentable.

Application No.: 10/761,992

Docket No.: JCLA11796

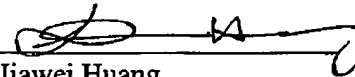
CONCLUSION

For at least the foregoing reasons, it is believed that the pending claims 1-7 and 12-15 are in proper condition for allowance. If the Examiner believes that a telephone conference would expedite the examination of the above-identified patent application, the Examiner is invited to call the undersigned.

Date: 10/21/2005

4 Venture, Suite 250
Irvine, CA 92618
Tel.: (949) 660-0761
Fax: (949)-660-0809

Respectfully submitted,
J.C. PATENTS



Jiawei Huang
Registration No. 43,330

"Exhibition A"

Modeling Refraction Characteristics of Silicon Nitride Film Deposited in a $\text{SiH}_4\text{-NH}_3\text{-N}_2$ Plasma Using Neural Network

Byungwhan Kim, Seung-Soo Han, Tae Seon Kim, *Member, IEEE*, Bum Soo Kim, and Il Joo Shim

Abstract—Silicon nitride has been deposited using plasma-enhanced chemical deposition (PECVD) equipment. The PECVD process was characterized by conducting a 2^{6-1} fractional factorial experiment on six experimental factors, including substrate temperature, pressure, radio frequency (RF) power, ammonia NH_3 , silane SiH_4 , and nitrogen N_2 flow rates. Refractive characteristics of the deposited film were examined by modeling the refractive index as a function of experimental factors. A helium-neon laser with a wavelength 6328 Å was used to measure the refractive index. To evaluate the appropriateness of the model, the network trained with 32 experiments was then tested with 12 experiments not pertaining to the training data. Several learning factors involved in training neural networks were optimized and an accurate prediction model with the root mean-squared error of 0.018 was achieved. Compared to statistical regression model, the neural network model demonstrated an improvement of more than 65%. Using various three-dimensional plots, underlying deposition mechanisms were qualitatively estimated. For the limited experimental ranges, the index increased with increasing SiH_4 flow rate. With an increase in either NH_3 or N_2 , meanwhile, the index decreased consistently. The index also increased with increasing substrate temperature or pressure. The effects of the temperature were very complex as it interacted with other factors.

Index Terms—Modeling, neural networks, plasma-enhanced chemical vapor deposition (PECVD), silicon nitride film.

I. INTRODUCTION

DEPOSITION of silicon nitride (SiN) film is one of the most critical processes that determine the efficiency of solar cells. The SiN film is widely used as the passivation layer for fabricating semiconductor devices due to the properties of good adherence and high resistance to migrating ions, moistures, surface oxidation. The SiN film is frequently deposited using plasma-enhanced chemical deposition (PECVD) [1]–[9]. PECVD of SiN is advantageous in that the film can be deposited

at lower substrate temperatures while yielding a good surface insulation. From the standpoint of manufacturing aspects, moreover, this technique provides such advantages as high throughput, good uniformity, and excellent reproducibility.

Film qualities of PECVD SiN depend on many experimental factors along with hardware variables. Predicting film properties is very important to their optimization as well as to gain insight into underlying deposition mechanisms. For plasma-driven processes, it has been a difficult task to construct prediction models due to complex particle interactions within a plasma. Analytical models basing on in-depth first principles are subject to many assumptions due to physical phenomena hard to understand and characterize. As a qualitative approach, neural networks have been applied to model pure plasma discharges [10], [11], chemical vapor deposition (CVD) process [12]–[17], and etch processes [18]–[28]. Neural network models demonstrated considerable improvement in prediction accuracy over statistical response surface models in modeling plasma [10], [29] and etch process [18]. Han *et al.* examined SiN film properties by constructing neural network models [12]. Although this study examined several process qualities simultaneously, it is somewhat limited in that very few aspects of each process quality could be revealed.

In this study, one important process quality—a refractive index—is exclusively studied in detail. The experimental data used here is the same as the previous one [12]. However, the predictive model constructed is much more accurate compared to previous models [12], [13]. This enables the SiN deposition process to be understood more clearly. Using the model, those aspects previously not examined are studied. The SiN film was deposited using a Plasma-Therm 700 series PECVD system in a $\text{SiH}_4\text{-NH}_3\text{-N}_2$ plasma [12]. The deposition process was characterized by a central composite-circumscribed (CCC) experimental design [30]. The experimental factors that were varied in the design include a substrate temperature, pressure, radio frequency (RF) power, NF_3 flow rate, SiH_4 flow rate, and N_2 flow rate. The refractive index was measured with a laser photoconductive decay (PCD) tester. The 32 experiments from the design including one center point were used to train neural network and trained network was tested on remaining 12 experiments for its appropriateness. Among many paradigms, the backpropagation neural network (BPNN) [31] was chosen for modeling due to its popularity in plasma process modeling. Effects of several important factors involved in network training were optimized systematically.

Manuscript received January 29, 2002; revised January 14, 2003. This work was supported by the Korea Research Foundation under Grant KRF-2002-041-D00117.

B. Kim is with the Department of Electronic Engineering, Sejong University, Seoul 143-747, Korea.

S.-S. Han is with the School of Information Control Engineering, Myongji University, Kyunggi-Do 449-7278, Korea.

T. S. Kim is with the School of Computer Science and Electronic Engineering, Catholic University of Korea, Bucheon 420-743, Korea (e-mail: tkim@catholic.ac.kr).

B. S. Kim is with the School of Electrical Engineering, Korea University, Seoul 136-701, Korea.

I. J. Shim is with the School of Information and Communication Engineering, Daeduk College, Daejeon 305-715, Korea.

Digital Object Identifier 10.1109/TPS.2003.812348

0093-3813/03\$17.00 © 2003 IEEE

TABLE I
EXPERIMENTAL FACTORS

Parameters	Range	Unit
Substrate Temperature	200-400	°C
Pressure	0.6-1.2	Torr
RF Power	20-40	Watts
NH ₃ Flow	1-1.4	sccm
SiH ₄ Flow	180-260	sccm
N ₂ Flow	0-1000	sccm

II. EXPERIMENTAL DETAILS

SiN films investigated in this study were deposited in a Plasma-Therm 700 series batch reactor operating at 13.56 MHz using NH₃, SiH₄, and nitrogen as feed gases. To characterize this process, it was employed the CCC experimental design consisted of 2^{6-1} fractional experiment and 12 axial points. One center point was also added. Those 32 experiments including one center point were used to train neural network. Prediction performance of trained network was then tested with the additional 12 experiments. The experimental factors that were varied in the design are included in Table I. Three-inch float zone p-type silicon wafers, with (100) orientation and a resistivity of 2.0 $\Omega\cdot\text{cm}$, were used as the substrates. During the deposition, SiH₄ was diluted to 2% in nitrogen. Approximately 0.05- μm silicon nitride was deposited. Refractive index to be modeled was measured by a helium-neon laser having a wavelength of 6328 Å.

III. FUNDAMENTALS OF NEURAL NETWORK

The BPNN architecture consists of three layers of neurons—input layer, hidden layer, and output layer. The input layer receives external information such as that represented by the six process parameters shown in Table I. The output layer transmits the data and, thus, corresponds to the various deposition responses. In this study, the number of neurons in the output layer was set to unity since one response was modeled. The BPNN also incorporates “hidden” layers of neurons that do not interact with the outside world, but assists in performing nonlinear feature extraction on the data provided by the input and output layers. Here, the number of the hidden layer was set to unity since this three-layered network is generally understood to learn arbitrary relationships between the input and output patterns.

The activation level (or firing strength) of a neuron is determined by a bipolar sigmoid function denoted as

$$\text{out}_{i,k} = \frac{1 - e(-\frac{\text{in}_{i,k}}{G_B})}{1 + e(-\frac{\text{in}_{i,k}}{G_B})} \quad (1)$$

where $\text{in}_{i,k}$ and $\text{out}_{i,k}$ indicate the weighted input to the i th neuron in the k th layer and output from that neuron, respectively. The G_B represents the gradient of the bipolar sigmoid function and determines the activation level of neuron. The BPNN adopted here uses a linear function in the output layer while maintaining the bipolar sigmoid function (1) in the hidden layer. This architecture has proven effective to

improving prediction accuracy of BPNN [32]. The linear function is expressed as

$$\text{out}_{i,k} = \text{in}_{i,k} \cdot G_L \quad (2)$$

where G_L represents the gradient of the linear function. For a given set of training factors, both gradients in (1) and (2) are to be optimized to improve the prediction accuracy.

The backpropagation (BP) algorithm by which the network is trained begins with a random set of weights (i.e., connection strengths between neurons). The Euclidean distance in the weight space the network attempts to minimize is the accumulated error (E) of all the input-output pairs, which is expressed as

$$E = \sum_{j=1}^q (d_j - \text{out}_j)^2 \quad (3)$$

where q is the number of output neurons, d_j is the desired output of the j th neuron in the output layer, and out_j is the calculated output of that same neuron. In BP algorithm, this error is to be minimized via the *gradient descent* optimization, in which the weights are adjusted in the direction of decreasing the E in (3). A basic weight update scheme, commonly known as the *generalized delta rule*, is expressed as

$$W_{i,j,k}(m+1) = W_{i,j,k}(m) + \eta \Delta W_{i,j,k}(m) \quad (4)$$

where $W_{i,j,k}$ is the connection strength between the j th neuron in the layer ($k-1$) and the i th neuron in the layer k , and $\Delta W_{i,j,k}$ is the calculated change in the weight to minimize the E in (3) and defined as

$$\Delta W_{i,j,k} = -\frac{\partial E}{\partial W_{i,j,k}} \quad (5)$$

Other parameters m and η indicate the iteration number and an adjustable parameter called “learning rate,” respectively. The η was set to 0.01 in this study. By adjusting the weighted connections recursively using the rule (4) for all the units in the network, the accumulated E for all training vectors is to be minimized.

IV. QUALITATIVE INTERPRETATION

A. Optimization of Neural Network Model

Many training factors are involved in optimizing prediction capability of neural network etch models [21], [29]. These include training tolerance, number of hidden neurons, gradients of activations functions, and magnitude of initial weight distribution. The training tolerance (T) determines the overall quality of the network modeling capability by specifying the accuracy of neuron outputs. At each training epoch, it is given by

$$T = \frac{\sum_{j=1}^h (d_j - \text{out}_j)^2}{k} \quad (6)$$

where k represents the total number of training vectors and it is 33 in this study. Complexity in optimizing the effects of training factors arises from random nature of initial weights. As reported in [29], this can partly be circumvented by generating multiple models for a given set of training factors. Each training factor

TABLE II
ESTIMATED REGRESSION COEFFICIENTS

Regression Coefficients	Fitted Coefficients
β_0	-0.963954
β_1	0.023132
β_2	-0.011257
β_3	-0.971635
β_4	0.321094
β_5	0.004569
β_6	-0.000265
β_7	0.000001
β_8	0.002417
β_9	-0.000500
β_{10}	-0.000009
β_{11}	0.0000002
β_{12}	0.003125
β_{13}	0.004063
β_{14}	0.000029
β_{15}	-0.000003
β_{16}	0.020833
β_{17}	0.000970
β_{18}	0.000042
β_{19}	-0.002227
β_{20}	-0.000038
β_{21}	0.000001
β_1^2	-0.000044

were experimentally varied for a fixed experimental range in a sequentially way. First, the training tolerance, hidden neurons, and initial weight distribution were varied and their optimal values found are 0.10, 6, and ± 0.5 , respectively. Prediction error of the refractive index model at these values is 0.0224. The prediction error quantified with the root mean-squared error (RMSE) metric was obtained from the test data, consisted of 12 axial points. The two gradients defined earlier were subsequently varied from 0.5 to 1.5 with an increment of 0.2 and from 0.5 to 2.5 with an increment of 0.4 for bipolar sigmoid and linear functions, respectively. A total of 36 combinations of gradients were, therefore, generated. For each combination, 200 multiple models were generated, of which one best model was then selected. Finally, one optimal model with the smallest RMSE was determined from 36 best models. The optimal model was obtained at the gradients of 0.7 and 1.3 for bipolar and linear functions, respectively. The corresponding RMSE of 0.018 demonstrates 19.2% improvement over the error obtained in the preceding optimization. As compared to the fuzzy logic model with the RMSE of 0.0448 appeared in [13], this illustrates 59.6% improvement. To compare with the statistical regression model, the refractive index data were fit to a quadratic polynomial expressed as

$$y = \beta_0 + \sum_{i=1}^k \beta_i x_i + \sum_{i=1}^k \beta_{ii} x_i^2 + \sum_{i,j} \beta_{ij} x_i x_j \quad (7)$$

where y is the etch response, β_i and β_{ij} are the regression coefficients, and x_i is the regressor variable corresponding to a process parameter. As stated earlier, an index k denotes the total number of process parameters. The estimated regression coefficients are contained in Table II. The RMSE of the regression

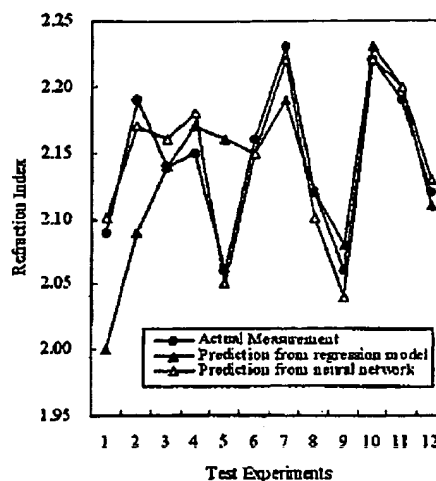


Fig. 1. Evaluation of prediction performance of neural network refractive index model.

model obtained is 0.052. Compared to the regression model, the neural network model, thus, exhibits about 65.3% improvement in the prediction accuracy. A significant improvement over fuzzy or statistical regression model is, thus, illustrated. With this high prediction accuracy, the characteristics of refractive index can, thus, be interpreted more clearly. To illustrate the accuracy of the model, the predictions from the models for 12 test experiments are compared to corresponding actual measurements in Fig. 1. As depicted in Fig. 1, neural network model yields better predictions at five cases (#1, #2, #5, #7, and #9). The improvement is conspicuous at three cases (#1, #2, and #5). At six cases (#4, #6, #7, #10, #11, and #12), their prediction capabilities seem to be comparable. In only one case (#3), the regression model is better than neural network counterpart. From this comparison, it is revealed that neural network model is superior to statistical model in prediction capability. By plotting various three-dimensional (3-D) plots from the predictive model constructed, behaviors of refractive index are examined qualitatively as a function of experimental factors.

B. Effects of SiH_4 and Substrate Temperature

Fig. 2 shows a refraction index versus SiH_4 and substrate temperature. The other RF power, pressure, NH_3 , and N_2 were set to 30 W, 0.9 torr, 1.2, and 500 sccm, respectively. As depicted in Fig. 2, the index increases linearly with an increase in SiH_4 flow rate at low 200 °C.

A simultaneous increase in either SiH or NH bond was observed from Fourier transform infrared spectroscopy (FTIS) [6]. The index increasing with SiH_4 flow rate in Fig. 2 can closely be correlated to increasing either Si/N [5] or SiH/NH bond ratio [6]–[8]. The effect of H content seems insignificant since at a relatively high ratio of SiH_4 with respect to NH_3 , the total hydrogen content remains almost constant. In the interpretation of Fig. 2, this is valid since the NH_3 flow rate in Fig. 2 was set to very small amount of 1.2 sccm. Meanwhile, Si-rich silicon nitride films showed poorer dielectric stability as illustrated by a decrease in the breakdown electric (E) field as well as the film

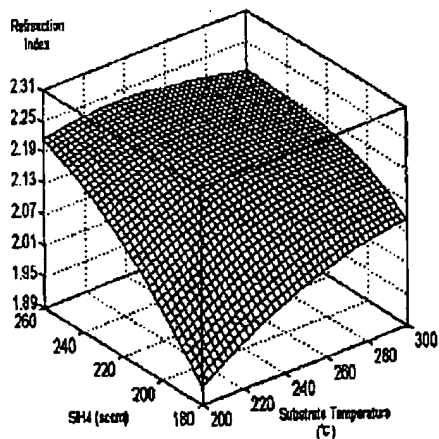


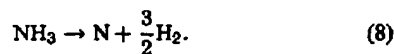
Fig. 2. Refractive index as a function of SiH₄ flow rate and substrate temperature.

insulation deteriorated due to relatively higher H content [7]. For the same variations in SiH₄ flow rate, the increase in the index is greatly suppressed at high 300 °C.

As seen in Fig. 2, the index increases with increasing the temperature at 180 sccm SiH₄. This can be explained by higher Si-N and lower H contents with an increase in the temperature [7]. At higher temperatures, the increase in the index seems weakened greatly. This is supported from the experimental data, in which the index initially increased considerably from 2.09 to 2.19 as the temperature increased from 200 °C to 250 °C at 220-sccm SiH₄. At the increased flow rate of 260 sccm, however, the index varies little with no consistency. This phenomenon has rarely been reported. This is mainly due to a shift in plasma condition, where the SH/NH ratio already increased appreciably at higher SiH₄ flow rate. As a result, refractive index is expected insensitive to variations in substrate temperature as the film contains fairly larger Si.

C. Effects of SiH₄ and NH₃

Fig. 3 plots a refraction index as a function of SiH₄ and NH₃. The other power, pressure, temperature, and N₂ were set to 30 W, 0.9 torr, 250 °C, and 500 sccm, respectively. The ratio of SiH₄ and NH₃ was once reported to have strong impact on the index [6]–[8]. Both SiH₄ and NH₃ are dissociated into radicals and atomic hydrogen, which passivate dangling bonds in silicon surface. A nitrogen (N) atom is deposited into the film from the NH₃ molecule by the dissociative adsorption, which is expressed as



As depicted in Fig. 3, the index linearly increases with an increase in SiH₄ at 1.4-sccm NH₃. As already explained, this is due to increased content of Si. This linear increase occurs over an entire range of NH₃. At the reduced 1-sccm NH₃, the index increases more conspicuously than at 1.4-sccm NH₃. Less N content at 1-sccm NH₃ is the main contributor to this phenom-

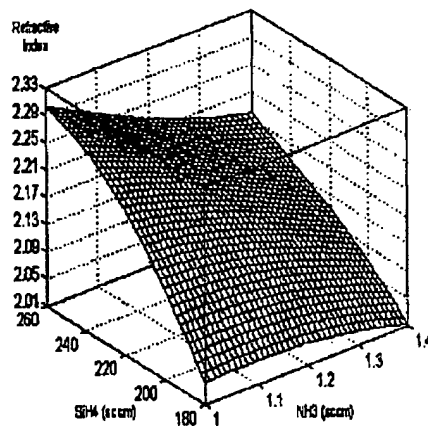


Fig. 3. Refractive index as a function of SiH₄ flow rate and NH₃ flow rate.

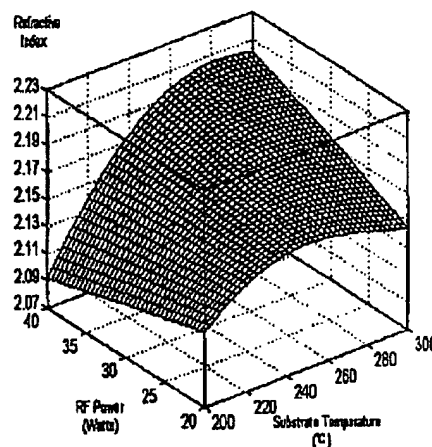


Fig. 4. Refractive index as a function of RF power and substrate temperature.

enon. In other words, the film incorporates higher Si content compared to N content.

As depicted in Fig. 3, the index varies very little with increasing NH₃ flow rate at 180 sccm SiH₄. When increasing the flow rate to a medium level of 220 sccm, the index then decreases noticeably with an increase in NH₃ flow rate. This is consistent with experimental data, in which the index decreased from 2.23 to 2.13. This phenomenon becomes more transparent at further increased flow rate of 260 sccm. This is mainly attributed to the N content, which has already been increased considerably by dissociating SiH₄ compared to that at lower 180 sccm. This implies that the NH₃ affects refractive index strongly at higher SiH₄. From the standpoint of device quality, N-rich SiN_x film results in better characteristics of thin film transistor.

D. Effects of RF Power and Substrate Temperature

Fig. 4 shows a refraction index as a function of RF power and substrate temperature. Other parameters were set to their default values. Namely, pressure, NH₃, SiH₄, and N₂ were set to 0.9

torr, 1.2, 220, and 500 sccm, respectively. As depicted in Fig. 4, the index initially increases with an increase in the temperature and then saturates. The temperatures at which the saturation begins are different depending on the level of power. As already reasoned, this increase stems from a higher S-N content and a lower H content. Also, the index remaining almost constant at extremely high temperatures can be reasoned well by referring to the experiments that increasing H flow resulted in an increase in Si-N ratio [9]. This implies that the decreased H content at higher temperatures led to a reduction in the Si/N ratio, thereby suppressing the increase of total Si/N ratio. The increase in the index at 40 W is more noticeable compared to that at 20 W. This is clear indicative that ion bombardment is involved in increasing refractive index.

At high temperature of 300 °C, as displayed in Fig. 4, the index increases with increasing RF power. This is because denser film is formulated at increased power, which in turn is induced by the removal of reaction byproducts much facilitated by enhanced ion bombardment. However, excessive ion bombardment can degrade surface passivation. This is partly supported from the experimental data for effective life time of the film measured with a laser PCD tester, which decreased from 58 to 56 with an increase in RF power from 20 to 40 W with other parameters set at their default values. At a mid-temperature of 250 °C, the index appears to vary little despite an increase in the power. This is in good agreement with the experimental data, in which the index increased from 2.14 to 2.15 only by 0.01 for the same increase in the temperature. In contrast to the index behavior at 300 °C, the index appears to decrease slightly with increasing power at low 200 °C. An illustrative example is that the index decreased from 2.12 to 1.71 with increasing power at the same 200 °C. The other pressure, NH_3 , SiH_4 , and N_2 were set to 1.2 torr, 1, 180, and 1000 sccm, respectively. A decrease in the Si-H-N-H can thus be expected, which is incurred by the film composition at 200 °C, with less Si-N bonds and higher H-content, as observed from Fig. 4, the index varied in a great complexity with RF power depending on the temperature. This is supported from a similar phenomenon once noticed in the Si-N ratio as a function of RF power [9].

E. Effects of Substrate Temperature and N_2 Flow Rate

Fig. 5 shows interaction effects of substrate temperature and N_2 flow rate on a refractive index. The other power, pressure, NH_3 , and SiH_4 were set to 30 W, 0.9 torr, 1.2, and 220 sccm, respectively. As already observed in Fig. 4, the index increases with increasing the temperature and then saturates to a constant value. Observing this behavior over an entire range of N_2 flow rate implies that the interaction effect of N_2 on the index is little as the temperature is varied. In contrast, the index decreases with an increase in N_2 flow rate. This behavior coincides with previous experiments [7] and can be supported from many experiments conducted in this study. As an illustration, the index at 250 °C decreased from 2.19 at to 2.12 with increasing the N_2 flow rate from 0 to 1000 sccm. This decreasing behavior is clearly represented on the corresponding response surfaces in Fig. 5. This decrease can be explained by the decreasing SH-NH

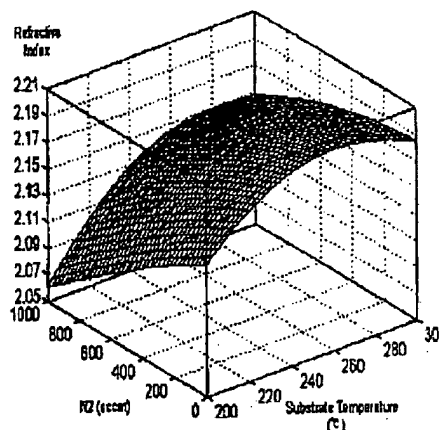


Fig. 5. Refractive index as a function of N_2 and substrate temperature.

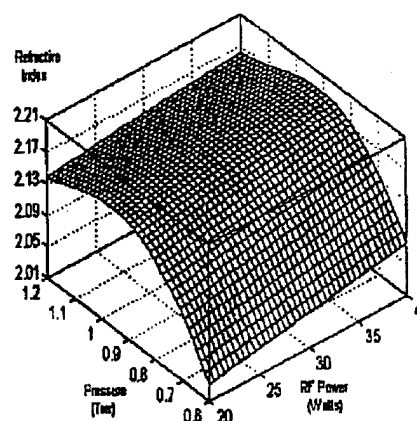


Fig. 6. Refractive index as a function of pressure and RF power.

ratio, which in turn is incurred by the increasingly absorbed N_2 content.

F. Effects of Chamber Pressure and RF Power

Fig. 6 depicts a refractive index as a function of chamber pressure and RF power. The other substrate temperature, RF power, NH_3 , and SiH_4 , and N_2 were set to 250 °C, 30 W, 1.2, 220, and 500 sccm, respectively. With increasing the pressure at low 20 W, the index initially increases drastically and then saturates. This exactly coincides with the behavior of experimental data, in which the index initially increased appreciably from 2.06 to 2.16 with increasing the pressure from 0.6 to 0.9 torr, and it then remained at 2.16 for further increase in pressure to 1.2. The increasing index is closely related to increased collision rate at high pressures, whereby the film is likely to deposit more regularly. Meanwhile, the increase in the index implies an increase in Si content. As depicted in Fig. 6, the index increases slightly with RF power, which is observed over an entire range of pressure. This is indicative that RF power affects the index independently of pressure.

V. CONCLUSION

Using neural networks, refractive index of silicon nitride films deposited in a plasma was modeled. A statistical 2^{6-1} fractional factorial experiment was conducted to characterize factor effects on the index. By optimizing training factors, very accurate prediction model was achieved as demonstrated from the comparisons with previous models. With reference to the relative contents of Si, N, or H, underlying deposition mechanisms were qualitatively estimated. Behaviors of the index with factors coincided with previous studies as well as some experiments performed here. The index behaved consistently with SiH_4 , N_2 , and NH_3 flow rates. However, RF power and substrate temperature showed complex behaviors depending on the levels of factors.

REFERENCES

- [1] C. Johnson, T. Wydeven, and K. Donohoe, "Plasma-enhanced CVD silicon nitride antireflection coatings for solar cells," *Solar Energy*, vol. 31, no. 4, pp. 355-358, 1983.
- [2] P. Michiels, L. Verhoef, J. Stroom, W. Sinke, R. van Zolingen, C. Denisse, and M. Hendriks, "Hydrogen passivation of polycrystalline silicon solar cells by plasma deposition of silicon nitride," *Proc. 21st IEEE Photovoltaic Specialists Conf.*, pp. 638-643, 1990.
- [3] M. Lemiti, J. Gervais, and S. Martinuzzi, "Hydrogenation of multicrystalline silicon from a backside silicon nitride layer," *Proc. 22nd IEEE Photovoltaic Specialists Conf.*, pp. 1002-1005, 1991.
- [4] Z. Chen, P. Sana, J. Salami, and A. Robatgi, "A novel and effective PECVD SiO_2/SiN antireflection coating for Si solar cells," *IEEE Trans. Electron Devices*, vol. 40, pp. 1161-1165, June 1993.
- [5] P. Temple-Boyer, L. Jalabert, L. Masarotto, J. L. Alay, and J. R. Morante, "Properties of nitrogen doped silicon films deposited by low pressure chemical vapor deposition from silane and ammonia," *J. Vac. Sci. Technol. A, Vac. Surf. Films*, vol. 18, no. 5, pp. 2389-2393, 2000.
- [6] J. Biemer, M. Jacob, and H. Schonherr, "Characterization of step coverage change in ultraviolet-transparent plasma enhanced chemical vapor deposition silicon nitride film," *J. Vac. Sci. Technol. A, Vac. Surf. Films*, vol. 18, no. 6, pp. 2843-2846, 2000.
- [7] M. Orfert and K. Richter, "Plasma enhanced chemical vapor deposition of SiN-films for passivation of three-dimensional substrates," *Surf. Coat. Technol.*, vol. 116-119, pp. 622-628, 1999.
- [8] K. Takechi, T. Takagi, and S. Kaneko, "The mechanism at work in 40 MHz discharge SiH_4/N_2 plasma chemical vapor deposition of SiNx at very high rates," *Jpn. J. Appl. Phys.*, vol. 37, pp. 1996-2001, 1998.
- [9] H. Gleskova, S. Wagner, V. G. parik, and P. Kovac, "Low-temperature silicon nitride for thin-film electronics on polyimide foil substrates," *Appl. Surf. Sci.*, vol. 175-176, pp. 12-16, 2001.
- [10] B. Kim and G. Park, "Modeling plasma equipment using neural networks," *IEEE Plasma Sci.*, vol. 29, pp. 8-12, Apr. 2001.
- [11] B. Kim and S. Park, "Characterization of inductively coupled plasma using neural networks," *IEEE Trans. Plasma Sci.*, vol. 30, pp. 698-705, Apr. 2002.
- [12] S. Han, "Modeling and optimization of plasma-enhanced chemical vapor deposition using neural networks and genetic algorithms," Ph.D. dissertation, Georgia Inst. Technol., Atlanta, GA, 1996.
- [13] P. Geisler, C. S. G. Lee, and O. S. May, "Neurofuzzy modeling of chemical vapor deposition process," *IEEE Trans. Semiconduct. Manufact.*, vol. 13, pp. 46-60, Feb. 2000.
- [14] C. Di Natale, E. Proietti, R. Diamanti, and A. D'Amico, "Modeling of APCVD-doped silicon dioxide deposition process by a modular neural network," *IEEE Trans. Semiconduct. Manufact.*, vol. 12, pp. 109-115, Feb. 1999.
- [15] M. Marwah and R. L. Mahajan, "Building neural network equipment models using model modifier techniques," *IEEE Trans. Semiconduct. Manufact.*, vol. 12, pp. 377-381, Aug. 1999.
- [16] X. A. Wang and R. L. Mahajan, "CVD epitaxial deposition in a vertical barrel reactor-process modeling and optimization using neural network models," *J. Electrochem. Soc.*, vol. 142, no. 9, pp. 3123-3132, 1995.
- [17] S. Venkateswaran, M. M. Rai, T. R. Govindan, and M. Meyyappan, "Neural network modeling of growth process," *J. Electrochem. Soc.*, vol. 149, no. 2, pp. 137-142, 2002.
- [18] C. D. Himmel and G. S. May, "Advantages of plasma etch modeling using neural networks over statistical techniques," *IEEE Trans. Semiconduct. Manufact.*, vol. 6, pp. 103-111, May 1993.
- [19] E. Rietman and E. Lory, "Use of neural networks in semiconductor manufacturing processes: An example for plasma etch modeling," *IEEE Trans. Semiconduct. Manufact.*, vol. 6, pp. 343-347, Nov. 1993.
- [20] Y. Huang, T. Edgar, D. Himmelblau, and I. Trachtenberg, "Constructing a reliable neural network model for a plasma etching process using limited experimental data," *IEEE Trans. Semiconduct. Manufact.*, vol. 7, pp. 333-344, Aug. 1994.
- [21] B. Kim and G. May, "An optimal neural network process model for plasma etching," *IEEE Trans. Semiconduct. Manufact.*, vol. 7, pp. 12-21, Feb. 1994.
- [22] —, "Reactive ion etch modeling using neural networks on a simulated annealing," *IEEE Trans. Comp. Packag. Manufact. Technol.*, vol. 19, pp. 3-8, Mar. 1996.
- [23] T. S. Kim and G. S. May, "Optimization of via formation in photosensitive dielectric layers using neural networks and genetic algorithms," *IEEE Trans. Electron. Packag. Manufact.*, vol. 22, pp. 128-136, Apr. 1999.
- [24] B. Kim, J. Sun, C. Choi, D. Lee, and Y. Seol, "Use of neural networks to model low temperature tungsten etch characteristics in high density SF_6 plasma," *J. Vac. Sci. Technol. A, Vac. Surf. Films*, vol. 18, no. 2, pp. 417-422, 2000.
- [25] S. Bushman, T. F. Edgar, and I. Trachtenberg, "Modeling of plasma etch systems using ordinary least squares, recurrent network, and projection to latent structure models," *J. Electrochem. Soc.*, vol. 144, no. 4, pp. 1379-1389, 1997.
- [26] B. Kim, S.-M. Kong, and B.-T. Lee, "Modeling SiC etching in $\text{C}_2\text{F}_6/\text{O}_2$ inductively coupled plasma using neural networks," *J. Vac. Sci. Technol. A, Vac. Surf. Films*, vol. 20, no. 1, pp. 146-152, 2002.
- [27] B. Kim and J. H. Park, "Qualitative fuzzy logic model of plasma etching process," *IEEE Trans. Plasma Sci.*, vol. 30, pp. 673-678, Apr. 2002.
- [28] B. Kim, K.-H. Kwon, and S.-H. Park, "Characterizing metal-masked silica etch process in a CHF_3/CF_4 inductively coupled plasma," *J. Vac. Sci. Technol. A, Vac. Surf. Films*, vol. 17, no. 5, pp. 2593-2597, 1999.
- [29] B. Kim and S. Park, "An optimal neural network plasma model: A case study," *Chemom. Intell. Lab. Syst.*, vol. 56, pp. 39-50, 2001.
- [30] D. C. Montgomery, *Design and Analysis of Experiments*. New York: Wiley, 1991.
- [31] D. E. Rumelhart and J. L. McClelland, *Parallel Distributed Processing*. Cambridge, MA: MIT Press, 1986.
- [32] B. Kim, W. Choi, and H. Kim, "Using neural networks with a linear output neuron to model plasma etch processes," in *Proc. Int. Symp. Industrial Electronics*, vol. 1, 2001, pp. 441-445.



Byungwhan Kim received the B.S. and M.S. degrees in electrical engineering from Korea University, Seoul, South Korea, in 1985 and 1987, respectively, and the Ph.D. degree from the School of Electrical and Computer Engineering, Georgia Institute of Technology, Atlanta, in 1993.

He was a Principal Technical Staff Member at Hyundai Electronics, Kyungki-Do, Korea, in 1996, a Postdoctoral Research Fellow and Integrated Process Systems Assignee at Korea University in 1998, and a Faculty Member at Chonnam National University, Kwangju, Korea, until 2000. He is currently an Assistant Professor of electronic engineering at Sejong University, Seoul, South Korea. His research interests include neurofuzzy modeling, optimization, diagnosis, and control of semiconductor processes.

Dr. Kim was a recipient of the Electronic Packaging Fellow Award from the IEEE CPMT Society and Motorola Graduate Fellowship. He is a member of the Korean Institute of Electrical Engineers and KICASE.



Seung-Soo Han received the B.S. and M.S. degrees in electrical engineering from Yonsei University, Seoul, Korea, in 1986 and the Ph.D. degree from the School of Electrical and Computer Engineering, Georgia Institute of Technology, Atlanta, in 1996.

He was a member of the Technical Staff at Hyundai Electronics, Incheon, Korea, in 1996 and a Faculty Member at Hyeosung Catholic University, Taegu, Korea, from 1997 to 1998. He is currently an Assistant Professor in School of Information Control Engineering, Myongji University, Kyunggi-Do,

Korea. His research interests include modeling and the optimization of semiconductor processes using neural networks and genetic algorithm.



Bum Soo Kim received the B.S. and M.S. degrees in electrical engineering from Korea University, Seoul, in 1987 and 1989, respectively. Since 1997, he has been working toward the Ph.D. degree at the same university.

From 1989 to 1998, he was a Senior Engineer at LG Industrial Systems, Anyang, Korea. His research interests include qualitative data modeling and multivariate process control.

Mr. Kim is a member of the Korean Institute of Electrical Engineers.



Tae Seon Kim (M'96) received the B.S. and M.S. degrees in electrical engineering from Inha University, Incheon, Korea, in 1991 and 1993, respectively, and the Ph.D. degree from the School of Electrical and Computer Engineering, Georgia Institute of Technology, Atlanta, in 1998.

He was a Postdoctoral Research Fellow at the Packaging Research Center, Georgia Institute of Technology, in 1999, and a Senior Research Engineer at Samsung Electronics, Yongin, Korea, from 1999 to 2001. He is currently a Faculty Member

with the School of Computer Science and Electronics Engineering, Catholic University of Korea, Bucheon, Korea. His research interests include modeling, optimization, and control of semiconductor manufacturing processes, as well as multichip modules, packaging technologies, and artificial intelligence.

Il Joo Shim received the B.S. and M.S. degrees in electrical engineering from Korea University, Seoul, in 1987 and 1989, respectively. He is currently working toward the Ph.D. degree at the same university.

From 1989 to 1999, he was a Senior Engineer at LG Industrial Systems, Anyang, Korea, where his activities included the design and development of distribution automation system (DAS). Since 2001, he has been a Research Professor with the School of Information and Communication Engineering, Daeduk College, Daejeon, Korea. His research interests include the application of artificial intelligence to complex systems.

**This Page is Inserted by IFW Indexing and Scanning
Operations and is not part of the Official Record**

BEST AVAILABLE IMAGES

Defective images within this document are accurate representations of the original documents submitted by the applicant.

Defects in the images include but are not limited to the items checked:

- ☐ **BLACK BORDERS**
- ☐ **IMAGE CUT OFF AT TOP, BOTTOM OR SIDES**
- ☐ **FADED TEXT OR DRAWING**
- ☐ **BLURRED OR ILLEGIBLE TEXT OR DRAWING**
- ☐ **SKEWED/SLANTED IMAGES**
- ☐ **COLOR OR BLACK AND WHITE PHOTOGRAPHS**
- ☐ **GRAY SCALE DOCUMENTS**
- ☒ **LINES OR MARKS ON ORIGINAL DOCUMENT**
- ☐ **REFERENCE(S) OR EXHIBIT(S) SUBMITTED ARE POOR QUALITY**
- ☐ **OTHER:** _____

IMAGES ARE BEST AVAILABLE COPY.

As rescanning these documents will not correct the image problems checked, please do not report these problems to the IFW Image Problem Mailbox.